Pharmaceutical Research, Vol. 22, No. 9, September 2005 (© 2005)
DOI: 10.1007/s11095-005-6155-x

Research Paper

Influence of Air Flow on the Performance of a Dry Powder Inhaler Using Computational and Experimental Analyses

Matthew S. Coates,[1,2] Hak-Kim Chan,[2,4] David F. Fletcher,[1] and Judy A. Raper[1,3]

Received January 14, 2005; accepted May 26, 2005

Purpose. The aims of the study are to analyze the influence of air flow on the overall performance of a dry powder inhaler (Aerolizer®) and to provide an initial quantification of the flow turbulence levels and particle impaction velocities that maximized the inhaler dispersion performance.
Methods. Computational fluid dynamics (CFD) analysis of the flowfield in the Aerolizer®, in conjunction with experimental dispersions of mannitol powder using a multistage liquid impinger, was used to determine how the inhaler dispersion performance varied as the device flow rate was increased.
Results. Both the powder dispersion and throat deposition were increased with air flow. The capsule retention was decreased with flow, whereas the device retention first increased then decreased with flow. The optimal inhaler performance was found at 65 l min^{-1} showing a high fine particle fraction (FPF) of 63 wt.% with low throat deposition (9.0 wt.%) and capsule retention (4.3 wt.%). Computational fluid dynamics analysis showed that at the critical flow rate of 65 l min^{-1}, the volume-averaged integral scale strain rate (ISSR) was 5,400 s^{-1}, and the average particle impaction velocities were 12.7 and 19.0 m s^{-1} at the inhaler base and grid, respectively. Correlations between the device flow rate and (a) the amount of throat deposition and (b) the capsule emptying times were also developed.
Conclusions. The use of CFD has provided further insight into the effect of air flow on the performance of the Aerolizer®. The approach of using CFD coupled with powder dispersion is readily applicable to other dry powder inhalers (DPIs) to help better understand their performance optimization.

KEY WORDS: CFD, computational fluid dynamics; DPI; dry powder aerosols; inhalation drug delivery.

INTRODUCTION

Currently, all the pharmaceutical dry powder inhalers on the market are "passive" devices, relying on the patient's inspiratory air flow to disperse the powder formulation into single particles or agglomerates small enough for inhalation into the lung. In reality, complete dispersion of the powder never occurs in these commercial products, which also exhibit large performance variations. Numerous empirical studies have shown that inhaler performance is strongly affected by both the maximum inspiratory flow rate (1–4) and the flow rate acceleration (5,6), however, an understanding of the influence of air flow at a fundamental level is lacking.

Inspiratory air flow through a dry powder inhaler controls both the turbulence levels generated in the device and the intensity of particle impactions, which are pivotal to the inhaler dispersion performance. It is hypothesized that critical turbulence levels and particle impaction velocities must exist at which the inhaler dispersion performance will be maximized; that is, above these critical levels, dispersion would not improve further. Inspiratory flow rate also controls the velocity of the air flow exiting the device, which affects the amount of powder deposition in the throat. Increased throat deposition reduces the overall inhaler performance (referring to the ability of the device to disperse drug agglomerates, taking into account capsule, device, and throat retention). Consequently, an optimal flow rate will exist at which the overall inhaler performance is maximized.

The aims of this study are to investigate the influence of air flow on the overall performance of a dry powder inhaler (Aerolizer®) and to provide an initial quantification of the flow turbulence levels and particle impaction velocities that maximized the inhaler dispersion performance.

METHODS

Computational fluid dynamics (CFD) analysis, using ANSYS CFX5.7 (7), was performed in conjunction with experimental powder dispersion analysis to determine how the performance of an Aerolizer® (Plastiape S.p.A., Osnago, Italy) varied when the device flow rate was increased. The study was performed at flow rates ranging from 30 to 120 l min^{-1}. A wide range of flow rates was chosen to cover the

[1] Department of Chemical Engineering, University of Sydney, Sydney, NSW 2006, Australia.
[2] Faculty of Pharmacy, University of Sydney, Sydney, NSW 2006, Australia.
[3] Department of Chemical Engineering, University of Missouri-Rolla, Missouri, USA.
[4] To whom correspondence should be addressed. (e-mail: kimc@pharm.usyd.edu.au)

full range of air flows attainable by a patient (1,8). Computational fluid dynamics analysis was performed to determine the nature of the flowfield experienced in the device at each flow rate. The performance of the inhaler was determined experimentally using mannitol powder and a multistage liquid impinger at the corresponding flow rate (see Dispersion Methodology). Mannitol powder aerosol has been used in bronchoprovocation testing for asthma and to enhance clearance of mucus in people who have excessive secretions (9–12).

Computational Methodology

The flowfield generated in the device at each flow rate was obtained by solving the Reynolds Averaged Navier Stokes equations together with the shear stress transport (SST) turbulence model (13) and automatic wall functions using the commercial CFD code ANSYS CFX 5.7 (7), as described in Coates *et al.* (14). The angular velocity of the capsule at each flow rate, required to model the motion of the rotating capsule, was determined using high-speed photography, as described in Coates *et al.* (15). Lagrangian particle tracking was performed as a postprocessing operation, in which the fate of 1,000 and 5,000 particles with a density of 1,520 kg m^{-3} (16) and particle diameter of 3.2 μm was tracked through the fluid after release from the capsule and subjected to drag and turbulent dispersion forces. By setting different walls within the device to have a zero coefficient of restitution, it was possible to determine the frequency and location of particle impactions at different sections of the device (namely, the inhaler base, grid, and mouthpiece, as indicated in Fig. 1). Modifications to the computational code were made to provide the speed and impact angle of all particles hitting the device walls. The same solution procedure as reported in (14) was employed.

Numerical studies were performed to ensure that the CFD results were independent of the computational mesh chosen. To obtain mesh-independent results, a series of five simulations was run in which the characteristics of the mesh applied to the geometry were varied significantly (Table I), increasing the total number of computational nodes by more than 110%. Coates *et al.* (14) have previously demonstrated mesh independence studies on the current computational mesh by analyzing the axial velocity profiles plotted throughout the device mouthpiece. However, to ensure that the turbulence properties obtained in this analysis were independent of the chosen mesh, volume-averaged values of the turbulence kinetic energy and integral scale strain rates were determined for each of the five meshes at each flow rate. As these quantities varied by less than 2% between the five cases (Table I), mesh independence of the computational results had been achieved.

The CFD models used throughout this study were validated using laser Doppler velocimetry (LDV) techniques by comparing the mouthpiece exit velocities obtained from the computational models with experimental data, as described in Coates *et al.* (14). Good agreement was observed between the computational and experimental results over a range of flow rates. In common with numerous other studies in this area, no validation of the levels of turbulence generated in the device or the interaction of particles with individual turbulent eddies has currently been performed. Therefore, the results in this study should be treated as a first quantification rather than as being definitive. However, despite this limitation, computational techniques similar to the one used throughout this study have been shown to be useful tools for interpreting complex experimental data (17–19).

Dispersion Methodology

The dispersion performance of the inhaler was determined using a four-stage (plus filter) liquid impinger (Copley, Nottinghamshire, UK), set up as described in the British Pharmacopoeia (20). For each dispersion, three hard vegetable capsules were filled with approximately 20 mg of spray-dried mannitol (particle size d_{50} = 3.2 μm, span $[(d_{90} - d_{10})/d_{50}]$ = 1.3) and dispersed into the impinger *via* a United States Pharmacopeia (USP) throat with uncoated interior. The impinger was run at the test flow rate for a total of 4 s using a timed valve. The runs were performed in triplicate to obtain mean values. Mannitol was assayed by high-performance liquid chromatography (Waters, Milford, MA, USA) using refractive index detection. Centrifuged samples (100 μl) were injected into a C18 Radial-Pak column with deionized water as the mobile phase running at a flow rate of 1 ml min^{-1} for 10 min. A calibration curve was constructed using standard solutions of mannitol, which allowed the mass of powder deposited on each stage of the impinger and the fine particle fraction to be determined. Throughout the dispersion analysis, the temperature and relative humidity of the laboratory were maintained at 20 ± 2°C and 55 ± 5%, respectively.

In this study, the fine particle fraction was defined as the mass fraction of particles smaller than 5 μm, referenced against either the total mass of powder loaded into

a Mouthpiece b Grid c Inhaler Base

Fig. 1. Schematic of the different sections of the Aerolizer® used when determining the frequency and location of particle–device impactions.

Table I. Summary of the Five Meshes Used to Study Mesh Independence of the Computational Results for the 60-l min^{-1} Case

	Mouthpiece mesh size (mm)	Inhaler base mesh size (mm)	Inhaler grid mesh size (mm)	Number of computational nodes ($\times 10^5$)	Turbulence kinetic energy (J kg^{-1})	Integral scale strain rates (s^{-1})
Mesh 1	0.6	0.5	0.2	4.00	6.0	5,110
Mesh 2	0.55	0.5	0.2	4.40	6.1	5,170
Mesh 3	0.5	0.45	0.2	5.25	6.0	5,050
Mesh 4	0.5	0.45	0.2	7.25	6.0	5,070
Mesh 5	0.45	0.45	0.2	8.80	6.0	5,020

The last two columns give the volume-averaged values of the important turbulence quantities and show their insensitivity to the mesh used.

(FPF_{Loaded}), or the total mass of powder emitted from (FPF_{Em}), the device. As the cut-off at each impinger stage varies with flow rate, interpolation of the cumulative undersize plot was used to determine the fine particle fraction. Values of the stage cut-off diameter were approximated as being inversely proportional to the square root of the air flow rate (21). The percentage recovery throughout the dispersion analysis was 100 ± 3%. Analysis of variance (ANOVA) tests were carried out with a probability of less than 0.05 considered statistically significant (Minitab 13).

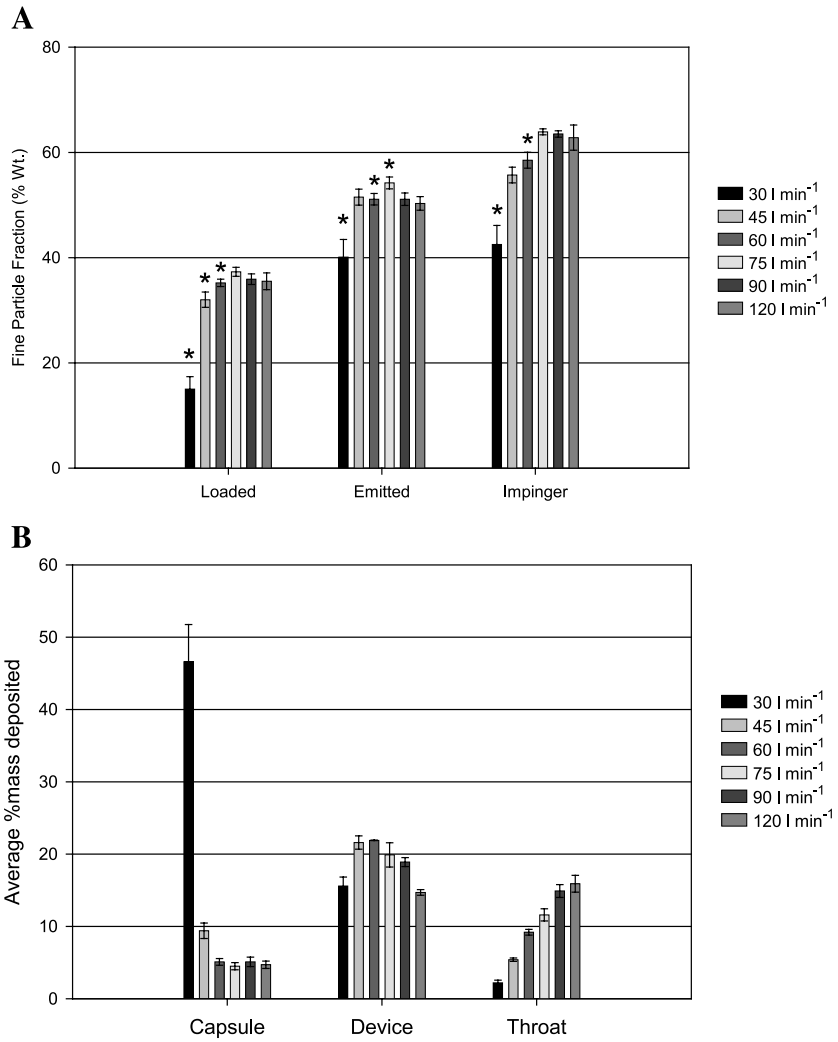

Fig. 2. (A) %FPF loaded, emitted, and impinger from the dispersion results performed to study the dependence of inhaler performance on flow rate (* denotes a statistically significant difference between the indicated and following result). (B) %Mass deposited at each location from the dispersion results performed to study the dependence of inhaler performance on flow rate.

Table II. Properties of the Device Flowfield at Each Test Flow Rate Used to Determine How the Deagglomeration Potential Varied with Flow Rate

Flow rate ($l\ min^{-1}$)	Velocity[a] ($m\ s^{-1}$)	Turbulence kinetic energy[a] ($J\ kg^{-1}$)	Integral scale strain rate[a] (s^{-1})	Mouthpiece exit velocity[b] ($m\ s^{-1}$)	Device pressure drop (Pa)
30	6.9	0.81	3,360	5.7	440
45	10.4	2.6	4,230	8.7	1,020
60	14.1	6.0	5,110	11.9	1,850
75	18.1	10.7	5,960	14.8	2,930
90	21.6	16.4	6,810	17.9	4,230
120	29.1	32.3	8,520	24.2	7,660

[a] Volume-averaged throughout the whole device.
[b] Area-averaged across the inhaler exit plane.

The FPF_{Loaded} and FPF_{Em}, which take into account powder retention in the capsule, device, and throat, are the conventional parameters used to determine the performance of a dry powder inhaler. In addition to these, the so-called "$FPF_{Impinger}$," defined as the fine particle fraction referenced against the mass of powder entering the multistage liquid impinger (stages 1–4, plus the filter), provides an alternative way of determining the inhaler dispersion performance. The $FPF_{Impinger}$ gives the particle size distribution and fine particle fraction occurring beyond the throat, providing useful information separate from the influence of capsule, device, and throat retention. Values of the FPF_{Loaded}, FPF_{Em}, and $FPF_{Impinger}$ will be used when discussing the results of this study.

RESULTS

Aerosol Characterization Results

The experimental powder dispersions showed that the inhaler displayed a poor performance at 30 l min^{-1}, where significantly lower FPF_{Loaded}, FPF_{Em}, and $FPF_{Impinger}$ values were produced (15.0, 40.1, and 42.5%, respectively) compared with all other flow rates (Fig. 2A). A significant performance increase was observed between 30 and 45 l min^{-1}, with the FPF_{Loaded}, FPF_{Em}, and $FPF_{Impinger}$ increasing to 32.0, 51.5, and 55.7%, respectively (Fig. 2A). Only minor differences in the FPF_{Loaded} and FPF_{Em} occurred above 45 l min^{-1}. A significant increase in the $FPF_{Impinger}$ was observed between 45 and 75 l min^{-1}, with the $FPF_{Impinger}$ increasing to 63.9%. No statistically significant differences in the $FPF_{Impinger}$ were observed between 75 and 120 l min^{-1}, indicating that above 75 l min^{-1}, no dispersion dependency with flow rate existed.

The amount of powder deposited in the throat after dispersion varied significantly with flow rate (Fig. 2B). At 30 l min^{-1}, throat deposition was 2.2%, which increased to 15.9% at 120 l min^{-1}. Statistically significant differences in the amount of throat deposition were observed between flow rate increase, except between 90 and 120 l min^{-1}. Increasing the device flow rate also led to a significant reduction in the mass of powder retained in the capsule (Fig. 2B). At 30 l min^{-1}, close to 50% of the loaded powder was retained in the capsule, compared with 9.4% at 45 l min^{-1} and 5.1% at 60 l min^{-1}. No further reduction in the amount of capsule retention was observed at flow rates greater than 60 l min^{-1}. Initially, the amount of device retention increased with flow rate, with the reverse trend occurring at flow rates greater than 60 l min^{-1} (Fig. 2B).

Computational Fluid Dynamics Results

Increasing the device flow rate from 30 to 120 l min^{-1} increased the values of the volume-averaged velocity from 6.9 to 29.1 m s^{-1} (Table II). As a result, a significant increase in the overall levels of turbulence generated in the device and the integral scale strain rates was observed (Table II). Increasing the device flow rate also had a strong effect on the inhaler exit velocity. The exit velocities (area-averaged over the entire exit plane) increased from 5.7 m s^{-1} at 30 l min^{-1} to 24.2 m s^{-1} at 120 l min^{-1} (Table II). The device pressure drop also increased significantly with flow rate, from 440 Pa at 30 l min^{-1} to 7,660 Pa at 120 l min^{-1} (Table II).

Table III summarizes the average particle impaction velocities that were observed on the different sections of the inhaler at flow rates of 30 and 120 l min^{-1}. The particle tracking was initially carried out to simulate the dispersion of 1,000 particles and repeated for 5,000 particles to determine if the particle impaction velocities obtained were independent of the number of particles simulated. No noticeable difference in the average particle impaction velocities was observed for the 5-fold increase in the number of particles, and therefore, the simulation of 1,000 particles was used with confidence for all other flow rates. Increasing the device flow rate increased the total number of particle impactions with the grid, mouthpiece, and inhaler base (Table IV). Additionally, the intensity of particle impactions increased significantly

Table III. Average Impact Velocity of Particle Collisions with the Different Sections of the Aerolizer® When the Computational Model Was Used to Simulate the Dispersion of 1,000 and 5,000 Drug Particles at 30 and 120 l min^{-1}

Flow rate ($l\ min^{-1}$)	Grid		Mouthpiece		Inhaler base	
	1,000	5,000	1,000	5,000	1,000	5,000
30	7.8	8.0	0.6	0.6	8.3	8.1
120	39.7	40.2	5.1	5.1	22.4	22.0

Table IV. Number and Average Impact Velocity of Particle Collisions with the Different Sections of the Aerolizer® When the Computational Model Was Used to Simulate the Dispersion of 1,000 Drug Particles Over the Full Range of Test Flow Rates

	Grid		Mouthpiece		Inhaler base	
Flow rate (l min^{-1})	Total impactions	Average impact velocity (m s^{-1})	Total impactions	Average impact velocity (m s^{-1})	Total impactions	Average impact velocity (m s^{-1})
30	1,276	7.8	880	0.6	322	8.3
45	1,345	12.0	1,950	1.3	1,162	9.9
60	1,285	17.6	4,880	1.8	2,450	11.9
75	1,319	24.1	6,850	3.0	3,846	13.5
90	1,402	29.4	7,977	3.3	4,688	16.1
120	1,545	39.7	10,013	5.1	6,130	22.4

between 30 and 120 l min^{-1} with the average particle impaction velocity increasing from 7.8 to 39.7 m s^{-1} for the grid, 0.6 to 5.1 m s^{-1} for the mouthpiece, and 8.3 to 22.4 m s^{-1} for the inhaler base (Table IV).

DISCUSSION

This study showed that increasing the air flow inhaled through a dry powder inhaler significantly changed the deagglomeration potential of the device flowfield and that these changes can have a strong effect on the inhaler performance. The deagglomeration potential is a term used to assess the ability of a device flowfield to disperse drug agglomerates, taking into account particle interaction with the turbulent flowfield and particle impactions with the device walls and neighboring particles. The scope of this study currently did not allow a determination into the intensity of particle–particle impactions; hence, this mechanism is not further discussed.

The results obtained from the CFD models showed that increasing the device flow rate significantly increased: (a) the overall levels of turbulence generated in the device; (b) the integral scale strain rates; and (c) the intensity and number of particle–device impactions. This combined effect increased the deagglomeration potential of the flowfield; hence, an improved dispersion was expected with flow rate. An increase in the inhaler dispersion performance occurred at each flow rate increment between 30 and 75 l min^{-1}, but no further improvement was observed above 75 l min^{-1}. Additional dispersion analysis showed that the dispersion plateau occurred at 65 l min^{-1} (Fig. 3). Analysis of the flowfield at this critical flow rate allowed us to determine turbulence levels and particle–device impaction intensities that maximized the inhaler dispersion performance.

The turbulence kinetic energy is a measure of the absolute turbulence level generated in the device, whereas the integral scale strain rate (defined as the turbulence eddy dissipation rate divided by the turbulence kinetic energy) is a measure of the velocity gradient across the integral scale eddies [the most energetic occurring in a turbulent flow (22)] and is hence a more appropriate parameter to study agglomerate breakup. The highest integral scale strain rates were generated in the lower region of the device, below a position approximately 2 mm upstream from the grid and would have the most significant effect on dispersion.

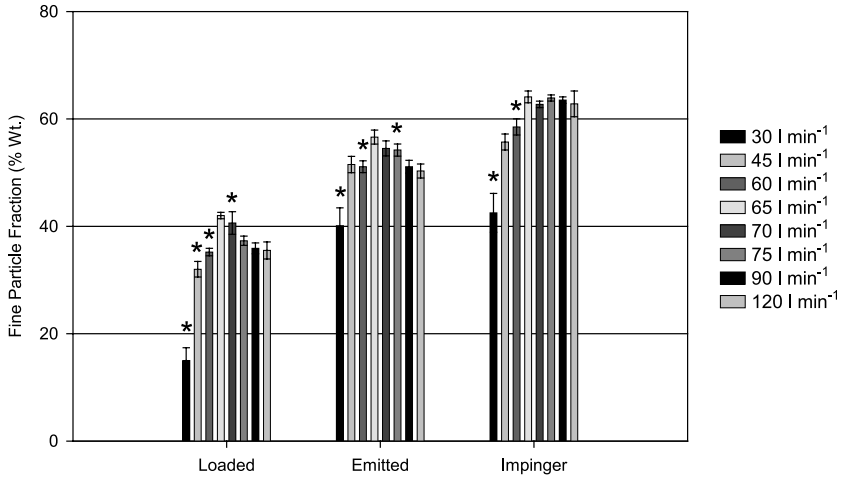

Fig. 3. %FPF loaded, emitted, and impinger from the original dispersion results (from Fig. 1a) with additional data at 65 and 70 l min^{-1}, performed to determine the flow rate at which the performance plateau occurred (* denotes a statistically significant difference between the indicated and following result).

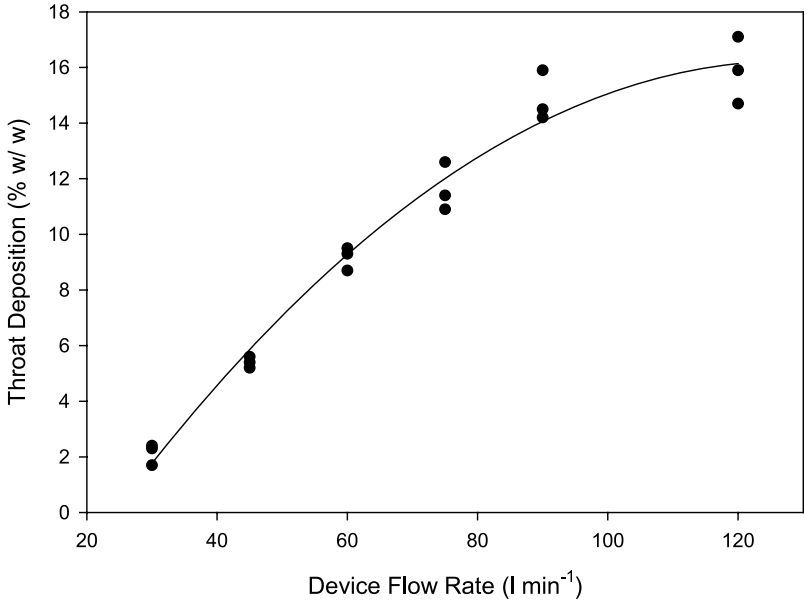

Fig. 4. A plot of throat deposition against device flow rate demonstrating that a clear relationship between throat deposition and device flow rate exists.

An increasing trend in the ISSR was observed with flow rate. At the critical device flow rate, a volume-averaged ISSR of 5,400 s^{-1} was generated in the inhaler base. Further increases in the integral scale strain rate did not improve dispersion.

Particle impactions with the grid and inhaler base occurred at significantly greater velocities than particle–mouthpiece impactions (Table IV); hence, these will have the most significant effect on agglomerate breakup. At the critical device flow rate, particle impaction velocities with the grid and inhaler base occurred at an average velocity of 19.0 and 12.7 m s^{-1}, respectively. The computational models used throughout this study could not determine which deagglomeration parameter (i.e., integral scale strain rates or particle impaction velocity) had the most significant effect on the inhaler dispersion performance.

Using a powder deagglomeration rig for experimental studies, Voss and Finlay (23) showed that mechanical impaction of the powder on a grid is not an effective breakup mechanism. Furthermore, they have shown that turbulence plays a definite, although not necessarily the dominant, role on fine particle dispersion. Although experimental rigs may be used to study powder deagglomeration, their design and dispersion mechanisms are not identical to that of dry powder inhalers, as discussed by the authors (14,15). Hence, further studies would be required to determine which

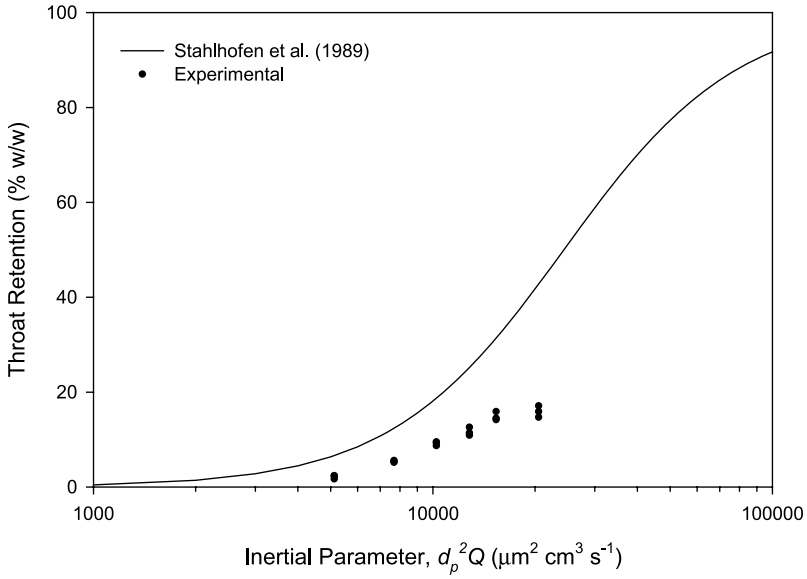

Fig. 5. A comparative plot of the throat deposition–inertial parameter relationship obtained experimentally with the semiempirical curve produced by Stahlhofen *et al.* This plot supports claims that the USP throat used in the MSLI seriously underestimates the amount of throat deposition for use with dry powder inhalers.

Table V. Dependence of the Capsule Emptying Time on Device Flow Rate Used to Explain Significant Differences in the Amount of Capsule Retention

Device flow rate ($l\ min^{-1}$)	30	45	60	75	90	120
Capsule emptying time (s) ($n = 3$)	10.5 ± 0.5	4.5 ± 0.25	2.25 ± 0.5	1.3 ± 0.1	0.85 ± 0.1	0.5 ± 0.05

mechanism (i.e., particle interaction with turbulence or particle–device impactions) has the most significant effect on agglomerate dispersion within dry powder inhalers.

This study has been performed to quantify integral scale strain rates and particle–device impaction velocities that occurred at a flow rate where the Aerolizer® dispersion performance was maximized. However, it is unclear whether these are the critical turbulence levels and particle impaction velocities required to maximize the performance of other dry powder inhalers. A fundamental study analyzing the device flowfield for a range of simplified geometries would be required to determine the critical levels and will form the basis of a future study. Furthermore, because powder breakup also depends on the cohesive strength of agglomerates, which cannot be sufficiently modeled using CFD, experimental study of the cohesive force [e.g., by atomic force microscopy (24,25)] coupled with other computational analyses such as discrete element method (26–28) would be necessary to obtain a more comprehensive understanding of powder deagglomeration for different drug formulations.

Figure 3 shows that the maximum FPF_{Loaded} and FPF_{Em} values also occurred at the critical device flow rate of 65 l min^{-1}. When studying the FPF_{Loaded} and FPF_{Em}, powder retention in the capsule, device, and throat need to be considered. At a flow rate of 65 l min^{-1}, the throat deposition (9.0 wt.%) and capsule retention (4.3 wt.%) were relatively low, whereas the inhaler dispersion performance was maximized, explaining the optimum FPF_{Loaded} and FPF_{Em} values.

The study showed a strong dependence of throat deposition on device flow rate. Increasing the device flow rate increased the velocity of the flow exiting the device, which caused the increased throat deposition. A good correlation between the amount of throat deposition, Γ (% w/w), and the device flow rate, Q (l min^{-1}), was observed (Fig. 4) where

$$\Gamma = -0.0015Q^2 + 0.384Q - 8.4 \quad (1)$$

This demonstrates that between flow rates of 30 and 120 l min^{-1}, the amount of *in vitro* throat deposition produced using the Aerolizer® can be estimated if the device flow rate is known.

The traditional variable used to generate throat deposition correlations is the inertial parameter $d_p^2 q$, where d_p is the particle diameter in μm and q is the device flow rate expressed in $cm^3\ s^{-1}$ (29). Comparing the throat deposition–inertial parameter relationship obtained experimentally from this study with the semiempirical curve produced by Stahlhofen *et al.* (30) (Fig. 5) supports claims that the USP throat used in the multistage liquid impinger (MSLI) seriously underestimates the amount of throat deposition for dry powder inhalers (31).

Figure 6 shows the existence of a linear relationship between the angular velocity of the capsule and device flow rate, where the capsule angular velocity, ω (in rpm), can be approximated by

$$\omega = 45Q \quad (2)$$

Studying the time taken for powder to empty out of the capsule, measured using a laser photometer as described in

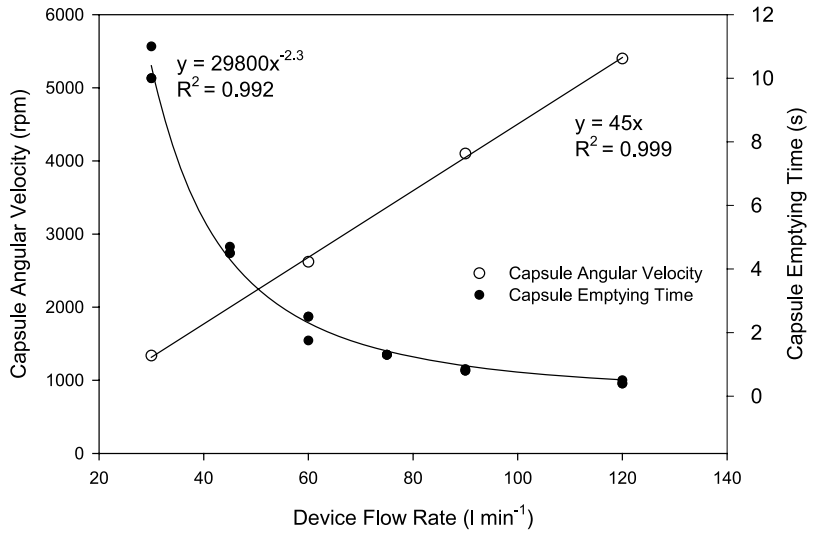

Fig. 6. Relationship between device flow rate, Q, and (a) capsule angular velocity, ω, and (b) capsule emptying time, t_{empty}, demonstrating that (i) the capsule angular velocity in the Aerolizer® can be approximated by $\omega = 45Q$ and (ii) the capsule emptying time can be approximated by $t_{empty} = 29{,}800Q^{-2.3}$.

Chew *et al.* (32) and Clark and Bailey (33), showed that increasing the device flow rate significantly reduced the capsule emptying time (Table V). A good correlation between the capsule emptying time, t_{empty} (s), and the device flow rate was observed (Fig. 6), where

$$t_{empty} = 29800Q^{-2.3} \quad (3)$$

At flow rates of 30 and 45 l min^{-1}, the time required to empty the capsule exceeded the 4-s impinger running time, accounting for the high capsule retention for these flow rates (Fig. 2B). Based on Eqs. (2) and (3), it can be shown that a capsule angular velocity of greater than 2,170 rpm would be required to empty the capsule (pierced using the four-pin piercing mechanism currently employed in the Aerolizer®) within the 4-s impinger run time.

At low flow rates, the amount of device retention increased with flow rate, with the trend reversing at flow rates greater than 60 l min^{-1} (Fig. 2B). The device retention was insignificant at low flow rates because of the reduced amount of powder exiting the capsule. Increasing the flow rate from 30 to 60 l min^{-1} increased the amount of powder exiting the capsule; hence, more was available to deposit on the device. The decreasing trend in device retention above 60 l min^{-1} was caused by the increase in the air velocities through the device. As the particle-surface detachment force is proportional to the square of the velocity (22), a greater detachment force was generated at higher flow rates, which resuspended a greater amount of particles temporarily deposited in the device. Coates *et al.* (14) reported that more than 90% of device retention occurred in the mouthpiece of the Aerolizer®, indicating that the velocities generated in the mouthpiece will have the most significant effect on particle resuspension. The present results suggest that a velocity of 5.0 m s^{-1} (generated in the inhaler mouthpiece at 60 l min^{-1}) is the critical velocity required to initiate particle detachment within the Aerolizer®.

CONCLUSIONS

The results showed that a critical flow rate of 65 l min^{-1} was required to maximize the Aerolizer® dispersion performance with the mannitol powder used. Analysis of the critical flowfield using CFD analysis has allowed us to determine the volume-averaged integral scale strain rates and average particle impaction velocities that maximized the inhaler performance. The maximum FPF_{Loaded} and FPF_{Em} values also occurred at the critical device flow rate of 65 l min^{-1} as the throat deposition (9.0 wt.%) and capsule retention (4.3 wt.%) were relatively low, whereas the inhaler dispersion performance was maximized.

Correlations between the device flow rate and (a) the amount of throat deposition and (b) the capsule emptying times have also been developed. The USP throat used in the multistage liquid impinger was found to seriously underestimate throat deposition for dry powder inhalers. It was also shown that a capsule angular velocity of greater than 2,170 rpm would be required to empty the capsule (pierced using the four-pin piercing mechanism currently employed in the Aerolizer®) within the 4-s impinger run time.

This work represents another step toward the fundamental understanding of the performance of dry powder inhalers and adds to our previous findings on the effect of design and the role of the capsule. The study methodology can be extended to other dry powder inhaler systems to provide vital information on optimal inhaler design.

ACKNOWLEDGMENTS

This work is funded by a grant from the Australian Research Council. Matthew S. Coates is a recipient of an International Postgraduate Research Scholarship. The authors would like to thank Plastiape S.p.A. for the supply of the inhalers.

REFERENCES

1. N. Y. K. Chew and H.-K. Chan. *In vitro* aerosol performance and dose uniformity between the Foradile Aeroliser and the Oxis Turbuhaler. *J. Aerosol Med.* **14**:495–501 (2001).
2. N. Y. K. Chew, D. F. Bagster, and H.-K. Chan. Effect of particle size, air flow and inhaler device on the aerosolisation of disodium cromoglycate powders. *Int. J. Pharm.* **206**:75–83 (2000).
3. N. Y. K. Chew and H.-K. Chan. Influence of particle size, air flow, and inhaler device on the dispersion of mannitol powders. *Pharm. Res.* **16**:1098–1103 (1999).
4. L. Borgström, H. Bisgaard, C. O'Callaghan, and S. Pedersen. Dry-powder inhalers. In H. Bisgaard, C. O'Callaghan, and G. C. Smaldone (eds.), *Drug Delivery to the Lung*, Marcel Dekker, Inc., New York, 2002, pp. 421–448.
5. A. H. de Boer, G. K. Bolhuis, D. Gjaltema, and P. Hagedoorn. Inhalation characteristics and their effects on *in vitro* drug delivery from dry powder inhalers. Part 3: the effect of flow increase rate (FIR) on the *in vitro* drug release from the Pulmicort 200 Turbuhaler. *Int. J. Pharm.* **153**(1):67–77 (1997).
6. V. Chavan and R. Dalby. Novel system to investigate the effects of inhaled volume and rates of rise in simulated inspiratory air flow on fine particle output from a dry powder inhaler. *AAPS Pharm. Sci.* **4**(2):Article 6 (2002).
7. ANSYS CFX (2003). www.ansys.com/cfx (accessed 08/01/04).
8. T. Meyer, P. Brand, H. Ehlich, R. Koebrich, G. Meyer, F. Riedinger, K. Sommerer, T. Weuthen, and G. Scheuch. Deposition of foradil P in human lungs: comparison of *in vivo* and *in vitro* data. *J. Aerosol Med.* **17**(1):43–49 (2004).
9. J. D. Brannan, S. D. Anderson, K. Gomes, G. G. King, H.-K. Chan, and J. P. Seale. Fexofenadine decreases sensitivity to and montelukast improves recovery from inhaled mannitol. *Am. J. Respir. Crit. Care Med.* **163**:406–412 (2001).
10. E. Daviskas, S. D. Anderson, K. Gomes, P. Briffa, B. Cochrane, H.-K. Chan, I. Young, and B. K. Rubin. Inhaled mannitol for the treatment of mucociliary dysfunction in patients with bronchiectasis: effect on lung function, health status and sputum. *Respirology* **10**:46–56 (2005).
11. S. D. Anderson, J. D. Brannan, and H.-K. Chan. Use of aerosols for bronchial provocation testing in the laboratory: where we have been and where we are going. *J. Aerosol Med.* **15**:313–324 (2002).
12. E. Daviskas, M. Robinson, S. D. Anderson, and P. T. P. Bye. Osmotic stimuli increase clearance of mucus in patients with mucociliary dysfunction. *J. Aerosol Med.* **15**:331–341 (2002).
13. F. R. Menter. Two-equation eddy-viscosity models for engineering applications. *AIAA J.* **32**:269–289 (1994).
14. M. S. Coates, D. F. Fletcher, H.-K. Chan, and J. A. Raper. Effect of design on the performance of a dry powder inhaler using computational fluid dynamics. Part 1: grid structure and mouthpiece length. *J. Pharm. Sci.* **93**:2863–2876 (2004).
15. M. S. Coates, H.-K. Chan, D. F. Fletcher, and J. A. Raper. The role of capsule on the performance of a dry powder inhaler using computational and experimental analyses. *Pharm. Res.* **22**(6):923–932 (2005).
16. P. G. Stecher, M. Windholz, and D. S. Leahy (eds.). *The Merck Index: An Encyclopedia of Chemicals and Drugs*, 8th edn., Merck & Co., Inc., Rahway, 1968.

17. E. A. Matida, W. H. Finlay, C. F. Lange, and B. Grgic. Improved numerical simulation of aerosol deposition in an idealized mouth–throat. *J. Aerosol Sci.* **35**:1–19 (2004).
18. E. A. Matida, W. H. DeHann, W. H. Finlay, and C. F. Lange. Simulation of particle deposition in an idealized mouth with different small diameter inlets. *Aerosol Sci. Tech.* **37**:924–932 (2003).
19. Y. Zhang, W. H. Finlay, and E. A. Matida. Particle deposition measurements and numerical simulation in a highly idealized mouth–throat. *J. Aerosol Sci.* **35**:789–803 (2004).
20. British Pharmacopoeia, Appendix XII, Aerodynamic assessment of fine particles—Fine particle dose and particle size distribution, Apparatus C (2001).
21. L. Asking and B. Olsson. Calibration at different flow rates of a multistage liquid impinger. *Aerosol Sci. Tech.* **27**:39–49 (1997).
22. W. H. Finlay. *The Mechanics of Inhaled Pharmaceutical Aerosols*, Academic Press Inc. Ltd., London, 2001.
23. A. Voss and W. H. Finlay. Deagglomeration of dry powder pharmaceutical aerosols. *Int. J. Pharm.* **248**:39–50 (2002).
24. P. Begat, D. A. V. Morton, J. N. Staniforth, and R. Price. The cohesive–adhesive balances in dry powder inhaler formulations I: Direct quantification by atomic force microscopy. *Pharm. Res.* **21**:1591–1597 (2004).
25. M. D. Louey and P. J. Stewart. Particle interactions involved in aerosol dispersion of ternary interactive mixtures. *Pharm. Res.* **19**:1524–1531 (2002).
26. R. Y. Yang, R. P. Zou, and A. B. Yu. Computer simulation of the packing of fine particles. *Phys. Rev. E.* **62**(3):3900–3908 (2000).
27. R. Moreno, M. Ghadiri, and S. J. Antony. Effect of the impact angle on the breakage of agglomerates: a numerical study using DEM. *Powder Technol.* **130**:132–137 (2003).
28. J. Subero, Z. Ning, M. Ghadiri, and C. Thornton. Effect of interface energy on the impact strength of agglomerates. *Powder Technol.* **105**:66–73 (1999).
29. B. Grgic, W. H. Finlay, P. K. P. Burnell, and A. F. Heenen. *In vitro* intersubject and intrasubject deposition measurements in realistic mouth–throat geometries. *J. Aerosol Sci.* **35**:1025–1040 (2004).
30. W. Stahlhofen, G. Rudolf, and A. C. James. Intercomparison of experimental regional aerosol deposition data. *J. Aerosol Med.* **2**:285–308 (1989).
31. W. H. Finlay, Y. Zhang, B. Grgic, A. Heenan, P. Burnell, E. A. Matida, A. Pollard, and C. F. Lange. Solving a major *in vitro–in vivo* correlation problem: impactor induction ports. In R. N. Dalby, P. R. Byron, J. Peart, J. D. Peart, and S. J. Farr (eds.), *Respiratory Drug Delivery IX*, Vol. I, Davis Healthcare Int. Publishing, River Grove, IL, 2004, pp. 203–209.
32. N. Y. K. Chew, H.-K. Chan, D. F. Bagster, and J. Mukhraiya. Characterization of pharmaceutical powder inhalers: estimation of energy input for powder dispersion and effect of capsule device configuration. *J. Aerosol Sci.* **33**:999–1008 (2002).
33. A. R. Clark and R. Bailey. Inspiratory flow profiles in disease and their effects on the delivery characteristics of dry powder inhalers. In R. N. Dalby, P. R. Byron, and S. J. Farr (eds.), *Respiratory Drug Delivery V*, Interpharm Press, Buffalo Grove, IL, 1996, pp. 221–230.